Optimization of struvite precipitation in synthetic biologically treated swine wastewater - Determination of the optimal process parameters

Aurélie Capdevielle, Eva Sýkorová, Béatrice Biscans, Fabrice Béline, Marie-Line Daumer

Optimization of struvite precipitation in synthetic biologically treated swine wastewater—Determination of the optimal process parameters

Aurélie Capdevielle[a,d,*], Eva Sýkorová[b], Béatrice Biscans[c], Fabrice Béline[a], Marie-Line Daumer[a]

[a] IRSTEA/Cemagref, 17 avenue de Cucillé, CS 64427, 35044 Rennes Cedex, France
[b] ICT Prague, Department Technology of water, Technická 5, Prague 6, 166 28, Czech Republic
[c] Université de Toulouse, Laboratoire de Génie Chimique, UMR 5503 CNRS/INP/UPS, Site de Labège, BP 84234, Campus INP-ENSIACET, 4 allée Emile Monso, 31030 Toulouse Cedex 4, France
[d] Université européenne de Bretagne (UEB), 5 Boulevard Laënnec, 35000 Rennes, France

HIGHLIGHTS

- Struvite precipitation is mainly influenced by the quantity of MgO added.
- Optimized parameters favoured struvite formation despite of high [Ca^{2+}] without adding other reagents.
- 90% of the total dissolved phosphorus is recovered as large crystals of struvite.
- Raman spectroscopy and solid dissolution show co-precipitation of ACP and presence of $CaCO_3$ in solid.

ABSTRACT

A sustainable way to recover phosphorus (P) in swine wastewater involves a preliminary step of P dissolution followed by the separation of particulate organic matter. The next two steps are firstly the precipitation of struvite crystals done by adding a crystallization reagent (magnesia) and secondly the filtration of the crystals. A design of experiments with five process parameters was set up to optimize the size of the struvite crystals in a synthetic swine wastewater. More than 90% of P was recovered as large crystals of struvite in optimal conditions which were: low Mg:Ca ratio (2.25:1), the leading parameter, high N:P ratio (3:1), moderate stirring rate (between 45 and 90 rpm) and low temperature (below 20 °C).These results were obtained despite the presence of a large amount of calcium and using a cheap reactant (MgO). The composition of the precipitates was identified by Raman analysis and solid dissolution. Results showed that amorphous calcium phosphate (ACP) co-precipitated with struvite and that carbonates were incorporated with solid fractions.

Keywords:
Struvite
P-recovery
MgO
Calcium phosphate
Swine wastewater
Raman

1. Introduction

The soil in Brittany (France) is extremely rich in phosphorus (P) because of intensive pig farming. P moves into surface waters due to soil erosion, and takes part in their eutrophication. Whilst needs of P as fertilizer increase every year, phosphate reserves are estimated to run out in 100 years [1]. P has to be recycled from our wastes. Therefore, some processes have been developed to recycle dissolved P as mineral fertilizer from urban wastewater. Calcium phosphate and struvite are the two forms of phosphate fertilizer produced. Struvite is known as a slow release fertilizer with comparable performances to, or even higher than, superphosphate from ore [2]. However, struvite recovery process, that recycles a significant amount of P, is seldom applied to concentrated effluents such as swine wastewaters. One of the limitations is the form that P actually presents in swine manure: 80% of P is in the particulate part [3].

A sustainable way to recover P in swine wastewater involves a preliminary step of P dissolution at pH 4.5 followed by the separation of residual particulate organic matter. Less reactant is needed when buffer effect is decreased by previously treating the effluent for nitrogen removal. The next two steps are: the precipitation of struvite crystals ($MgNH_4PO_4{\cdot}6H_2O$) by adding a crystallization reagent (magnesia, MgO) and the filtration of struvite crystals in filter bags with a 100 μm cut-off [4].

MgO was chosen as the precipitation reagent as its cost is low, it is a by-product from the animal food industry, it is safe and it fits to agricultural restrictions. It has two main functions: to increase

* Corresponding author at: IRSTEA/Cemagref, 17 avenue de Cucillé, CS 64427, 35044 Rennes Cedex, France.
E-mail addresses: aurelie.capdevielle@irstea.fr (A. Capdevielle), eva.sykorova@vscht.cz (E. Sýkorová), beatrice.biscans@ensiacet.fr (B. Biscans).

the pH value (6.5–11) and to get a molar ratio of Mg:N:P equal to 1:1:1 in order to reach the conditions to precipitate struvite in the solution [5,6]. Nevertheless, the control of the pH value and the molar ratio of Mg:Ca cannot be controlled independently of each other.

The control of the mechanisms of precipitation is the main issue to obtain: high value-added products, predictable mineral composition and big struvite crystals.

The amount and size of crystals depend on nucleation rate and crystal growth. These two mechanisms have already been modelled [7,8]. Nucleation rate is described by (1).

$$J_{1,hét}[\text{nb m}^{-3}\,\text{s}^{-1}] = A_{1,hét}\exp\left(-f.\Phi_v\frac{V_m^2\gamma_{g,l}^3}{(kT)^3\ln^2\beta}\right) \quad (1)$$

$$\beta = \frac{a_{Mg^{2+}}\times a_{NH_4^+}\times a_{PO_4^{3-}}}{K_{struvite}} \quad (2)$$

$$SI = \log(\beta) \quad (3)$$

$A_{1,het}$ is the nucleii agglomeration rate ($nb.m^{-3}.s^{-1}$), V_m is the nucleii molar volume (m^3), k the Boltzmann constant = 1.38×10^{-23} J.K^{-1}, T the temperature (K), $\gamma_{g,l}$ the nuclei/liquid interfacial energy ($N.m^{-1}$), β the supersaturation (2) and f and Φ_v are shape factors. a_i are the ion activities and $K_{struvite}$ is the solubility product of the struvite. SI (3), the saturation index is used to predict the precipitation potential of struvite. β is strongly dependant on the pH due to the dissolution of MgO, to the pK_a of the triprotic phosphoric acid (2.12, 7.21 and 12.67 at 25 °C) and the pK_a of NH_3/NH_4^+ (9.25).

The growth rate of a crystal is described by a two step model: the transport of the solutes to the crystals and their integration into the crystal structure [7–10].

The diffusion-controlled (G_d), the integration-controlled (G_r) and the overall linear growth rate (G_g) are described by the following equations (4), (5), (7) [7–9]. G_g is the sum of G_d and G_r and can be expressed in function of the mass flux density (dm/dt) (7).

$$G_d = \frac{L\times A}{3\times V_p\times\rho_c}\times k_d\times(c-c_i) \quad (4)$$

$$G_r = \frac{L\times A}{3\times V_p\times\rho_c}\times k_r\times(c_i-c*)^r \quad (5)$$

$$k_r = k_{r0}\times\exp\left(-\frac{\Delta E_r}{RT}\right) \quad (6)$$

$$G_g = \frac{L\times A}{3\times V_p\times\rho_c}\times k_g\times(c-c*)^g = \frac{L}{3\times V_p\times\rho_c}\times\frac{dm}{dt} \quad (7)$$

Where k_d (4) is the mass transfer coefficient, k_r (6) is the reaction rate constant, k_g is the growth rate constant, r is the order of the integration reaction, k_{r0} is the reaction constant, ΔE_r is the activation energy and g (7) is the overall order of the growth process (g = 1 at high supersaturation and 2 at low supersaturation). c, c_i and c* are the concentration of the solute, its concentration at the crystal-solution interface and its supersaturated concentration respectively. $c - c_i$ is the driving force for diffusion and $c_i - c^*$ is the driving force for reaction. L is the average diameter of the crystal; A is the area of the particle, V_p its volume and ρ_c the crystal density; m is the mass of the struvite formed.

In a continuous reactor, the struvite growth seems to follow a size dependent growth model [11]: the larger the crystals are, the faster the crystal grows. Nucleation and growth mechanisms are strongly dependent on pH, supersaturation, temperature, ionic strength of solution, presence of foreign substances, design of crystallizer, stirring, residence time of crystals [7,8]. When the influent contains both calcium and magnesium, a pH range of 7 to 11 enables the precipitation of both struvite and calcium phosphate [12–16].

Table 1
Ionic concentrations of synthetic and real effluents.

Ionic concentrations (mg L^{-1})	Real effluent	Synthetic effluent
Na^+	524 ± 163	2083 ± 152
K^+	1993 ± 453	1559 ± 120
Mg^{2+}	361 ± 35	345 ± 19
Ca^{2+}	694 ± 108	645 ± 38
Cl^-	1277 ± 262	2198 ± 40
NO_2^--N	356 ± 87	293 ± 3
NO_3^--N	68 ± 10	115 ± 2
PO_4^{3-}-P	654 ± 232	629 ± 3
SO_4^{2-}-S	113 ± 31	111 ± 1

Competition between the two products will depend on several factors amongst which the Mg:Ca and N:P molar ratios [17–19].

Most of the studies [20–22] on struvite and calcium phosphate crystallization have been performed on pure synthetic medium containing only the ions directly involved in their composition. Real influents have also been studied but with lower ionic strength compared to the swine wastewater after P dissolution. In these studies, magnesium and pH increase were usually provided by soluble reactants [21,23,24]. Magnesia dissolution kinetic and ammonia volatilization were not taken into account while they do determine the Mg:Ca and N:P molar ratios.

This study focuses on the influence of the process parameters on the precipitation of struvite in complex medium like swine wastewater. Precipitation was carried out in synthetic medium with an ionic composition close to the acidified swine slurry entering the crystallization step of the process. The purpose was to improve the precipitation of struvite instead of calcium phosphate in a stirred batch reactor. The studied process parameters were stirring rate, temperature, Mg:Ca and N:P molar ratio. A design of experiments was set up to understand the influence of these variables over struvite precipitation and crystal size. The surface response was employed to optimize the quantity of large crystals of struvite.

2. Experimental

2.1. Synthetic swine wastewater preparation

40 L of synthetic swine wastewater were prepared by mixing different salts in distilled water to obtain the ionic concentrations observed in the studied swine wastewater (Table 1). Formic acid (85%, Carlos Erba) was added in the solution until pH reached 4.5.

The salts used for synthetic effluent preparation were: KOH, K_2SO_4, $NaNO_2$, KNO_3, $CaCl_2{\cdot}2H_2O$ (Carlo Erba), $MgCl_2{\cdot}6H_2O$ and $Na_3PO_4{\cdot}12H_2O$ (Merck).

The ionic concentrations of synthetic swine wastewater were controlled by ion chromatography on Dionex DX-120. Concentrations for synthetic and real effluents are shown in Table 1.

The addition of a variable amount of NH_4Cl powder (99%, Carlo Erba) was performed 5 min before the beginning of each run to minimize the possible volatilization of NH_3. The addition was performed under high stirring.

2.2. Magnesia suspension

Previous experiments (data not shown) showed that a suspension of MgO in water was much more effective than MgO powder directly introduced into the reactor. MgO suspension was better dispersed and its reactivity was improved. This kind of suspension was also used in a similar study by Münch et al. [25]. The MgO suspension was prepared by mixing 500 g of MgO powder (97%, VWR Prolabo) in 5 L of distilled water. Magnesia was kept in suspension under continuous stirring at 300 rpm and was thermostated at the

same temperature as the runs. The runs began when adding the suspension of MgO.

2.3. Equipment

The runs were performed in a FC6s flocculator from Velp Scientifica. Six axial mixing blades are operated by six motors with various stirring rates from 10 to 200 rpm. Each beaker was filled with 800 mL of synthetic effluent. The addition of MgO was carried out under continuous stirring at 90 rpm for 30 s. Then, the stirring rate was maintained at the consigned value during 24 h. The runs were carried out in vessels thermostated by water circulating through a constant temperature bath (5 °C, 20 °C or 35 °C). pH and temperature were recorded by a 8 channels data logger PH/MV/ION/O2 from Fisher Scientific.

2.4. Sampling

Samples (4 mL) were collected from beakers every 30 min during 4 h and then after 24 h for dissolved compound analysis. At 4 h and 24 h, a 250 mL sample was collected for particle analysis.

After 24 h, samples were sieved on 25 and 100 μm filters. The three solid fractions (<25 μm, 25–100 μm and >100 μm) were dried at room temperature. Each fraction was then weighed and analyzed as described below.

2.5. Analysis

The composition of the collected fractions were analyzed by ion chromatography after solid dissolution by formic acid and by Raman spectroscopy. The precipitation rate was evaluated by monitoring the dissolved concentrations of Ca^{2+}, PO_4^{3-}, Mg^{2+} and NH_4^+.

2.5.1. Ionic concentration

The concentrations of dissolved PO_4-P, NH_4-N were analyzed by automate colorimetric methods on QuikChem® FIA+ from Lachat Instruments with QuikChem method 10-115-01-1-P and 10-107-06-1-J respectively. The dissolved Mg^{2+} and Ca^{2+} were determined by cation chromatography.

The three solid fractions were acidified with formic acid (85%, Carlo Erba) and diluted in 50 mL of distilled water. They were analyzed by cation and anion chromatography on Dionex DX-120 with an IonPac™ CS12A column and an IonPac™ AS9-HC column respectively.

The molar balance was checked by analysing the solid and liquid composition at the beginning and the end of the run.

2.5.2. Raman spectroscopy

Analysis were carried out at room temperature using a Raman microscope (Kaiser Optical Systems, Leica DM1) equipped with a thermoelectrically cooled CCD detector coupled to the spectrometer with multi-mode fibre optic cables; 50 μm diameter was employed for excitation, and 62.5 μm diameter for collection. The excitation of Raman scattering was operated by a 400 mW diode laser operating at 785 nm, with an average power output of 100–200 mW through an objective lens with a magnification of 20 X and a working distance of 11 mm. The spot size of the laser beam through the objective was approximately 20 μm. About 1 mg of solid was introduced on a microscope slide. The microscope was focused visually, using a white light source to maximize the Raman signal. The collection range was 100–3100cm^{-1}. The time of collection was then adjusted at 2 min in order to obtain a good signal-to-noise ratio.

2.6. Experimental design

The response surface plan used is a Box–Behnken modified plan with 48 runs: 12 centre points and one repetition for the extremities. Five process parameters were studied: A, the stirring rate, B, the temperature, C, the N:P molar ratio, D, the initial Mg:Ca molar ratio and E, the concentration of magnesium remaining as MgO particles.

D and E were originally grouped in one parameter: the Mg:Ca molar ratio. However, the measurement of dissolved Mg^{2+} in the MgO suspension showed variations at the beginning of each block of runs. To better describe the results and understand the effects, MgO was considered as two parameters for statistical treatment of the experimental data: the initial dissolved Mg:Ca ratio and the remaining Mg^{2+} as MgO, [Mg-MgO]. These two parameters were calculated from the dissolved Mg^{2+} measures in MgO suspension. The correlation matrix of the experimental design showed that, even with this change, there was no risk of confusion.

The design matrix and experimental level of each variable are described in

Table 2. The studied responses were: ionic concentrations (Ca^{2+}, PO_4^{3-} and NH_4^+) after 24 h, the production of particles >100 μm and the proportion of struvite versus calcium phosphate in dried solids.

2.7. Data evaluation

The Box–Behnken modified plan uses a second order polynomial model (8) to predict the ionic concentration values as a function of a combination of the process parameters (stirring rate, initial dissolved Mg: Ca ratio, [Mg-MgO], N:P ratio and temperature) [26].

$$Y = \beta_0 + \sum_{i=1}^{5}\beta_i X_i + \sum_{i<j}\beta_{ij} X_j + \sum_{i=1}^{5}\beta_{ii} X_i^2 + \varepsilon \quad (8)$$

Where Y is the predictive response. In this paper, six responses were predicted and five were used for the optimization step. β_0 is the constant term. β_i are the coefficients of the linear parameters X_i (A, B, C, D, E). β_{ij} represents the coefficients of the interaction parameters X_i and X_j (for instance: AB, AC, AD...). β_{ii} represents the coefficients of the quadratic parameters X_i^2 (AA, BB, CC, DD and EE) which show the quadratic dependence of the responses to a parameter.

Statgraphics Centurion XVI, 16.1.11 software was used for experimental design and data evaluation. The statistical models are said to fit the experimental data when the adjusted R^2 were greater than or equal to 65%. A low probability F value ("Prob. > F") less than 0.05 indicates process parameters are significant.

2.8. Determination of the final solid phases by PHREEQC®

The saturation index (SI) of the various minerals was calculated using the geochemical software PHREEQC® with the Minteq.V4 database. The database was modified to include the struvite and amorphous calcium phosphate (ACP) phases. The K_{sp} values for struvite were adapted to the temperature of the runs according to Hanhoun et al. [27]. The K_{sp} value for ACP was set at 26.83, the mean value of the K_{sp} for ACP from all the studies described by Mañas et al. [28]. The Ksp for brucite was set at 17.01 according to the study of Altmaier et al. [29].Several minerals were removed from the database as they cannot precipitate through the conditions of the runs: the monetite ($CaHPO_4$), the magnesite ($MgCO_3$), the aragonite ($CaCO_3$), the dolomite ($CaMg(CO_3)_2$, the huntite ($Mg_3Ca(CO_3)_4$), the β-tricalciumphosphate ($Ca_3(PO_4)_2$) as they can only form at high temperature [30,31], the hydroxyapatite ($Ca_5(PO_4)_3(OH)$) and the octocalciumphosphate (OCP, $Ca_8(HPO_4)_2(PO_4)_4{\cdot}5H_2O$) as

Table 2
The modified Box–Behnken design for optimization of 5 variables each at three levels.

Runs	Stirring rate (rpm)	Initial Mg:Ca molar ratio	[Mg-MgO] (mg L^{-1})	N:P molar ratio	Temperature (°C)
Low	10	0.63	475	0.71	5
Middle	45	1.06	1 228	2.03	20
High	90	1.66	2 617	3.11	35
1	10	1.08	475	2.86	5
2	45	1.10	475	1.96	5
3	90	1.59	797	2.00	5
4	10	1.66	797	1.00	5
5	10	1.66	797	3.00	5
6	45	1.57	797	2.00	5
7	45	0.84	1 607	2.00	5
8	45	1.11	975	2.00	5
9	45	1.14	1 606	2.00	5
10	45	1.09	975	3.00	5
11	45	1.09	975	2.00	5
12	90	0.71	975	3.00	5
13	10	1.02	1 657	2.00	20
14	10	1.09	1 026	3.00	20
15	10	1.11	1 026	2.13	20
16	45	1.02	500	1.03	20
17	45	0.99	1 044	2.14	20
18	45	1.00	1 044	1.00	20
19	45	1.13	991	1.89	20
20	90	1.15	991	2.31	20
21	45	0.91	1 004	0.90	20
22	45	1.02	1 635	2.35	20
23	45	1.08	1 004	2.20	20
24	45	1.07	478	2.15	20
25	45	0.81	1 052	2.14	20
26	45	0.80	1 683	2.10	20
27	45	1.05	1 052	1.93	20
28	90	0.80	1 052	1.95	20
29	90	0.92	552	1.92	20
30	45	0.95	1 085	2.14	20
31	45	0.63	552	2.14	20
32	45	0.85	1 085	2.89	20
33	45	0.90	1 087	2.25	20
34	90	0.91	1 718	2.14	20
35	45	0.97	1 087	2.13	20
36	45	0.85	1 087	1.19	20
37	10	0.94	1 637	2.48	35
38	90	0.90	1 637	0.71	35
39	45	1.00	2 608	2.86	35
40	45	1.00	1 160	1.96	35
41	45	0.94	872	2.00	35
42	45	0.96	1 637	1.00	35
43	90	1.18	1 613	3.00	35
44	10	1.18	1 613	2.00	35
45	45	1.43	2 618	2.00	35
46	45	1.30	2 159	2.00	35
47	45	1.35	2 324	2.00	35
48	45	1.18	2 324	3.00	35

according to the Ostwald's rules, the less stable forms (amorphous calcium phosphate (ACP) or dicalcium phosphate dihydrate (DCPD, $CaHPO_4{\cdot}2H_2O$)) precipitate first [7,12,32,33]. The SI values were calculated using the initial concentrations. The concentration of Mg^{2+} was defined by the total Mg potentially dissolved. The concentration of carbonates adjusted the charge balance. When SI > 0 (>0.5 with the security margin [28]), the supersaturation is reached and minerals are able to precipitate.

3. Results and discussions

The experimental design evaluates the influence of process parameters on P-recovery as large struvite crystals.

In each run, the molar balances were controlled for phosphorus, nitrogen, calcium and magnesium. Each molar balance was a sum of 4 or 5 analytical data. The ammonia volatilization was calculated thanks to the liquid/solid molar balance for ammonium (12) in part 3.1.3. Errors in molar balance were below the sum of experimental errors.

3.1. Phosphate removal considering ammonia volatilization

3.1.1. Phosphate removal is mainly influenced by stirring rate and addition of MgO

The evolution of the phosphate concentration follows a first order kinetic (9) [34].

$$-\frac{d[PO_4-P]_t}{dt} = K([PO_4-P]_t - [PO_4-P]_e) \quad (9)$$

The expression of $[PO_4\text{-}P]_t$ (10) is the result of the integration of (9).

$$[PO_4-P]_t = ([PO_4-P]_e - [PO_4-P]_0) \times (1-e^{-Kt}) + [PO_4-P]_0 \quad (10)$$

Where $[PO_4\text{-}P]_t$ is the concentration of the totally dissolved phosphate at t. $[PO_4\text{-}P]_0$ and $[PO_4\text{-}P]_e$ are the concentration before the addition of MgO and at equilibrium respectively. K is a kinetic constant. For runs at 10 rpm, the concentrations of the final PO_4-P

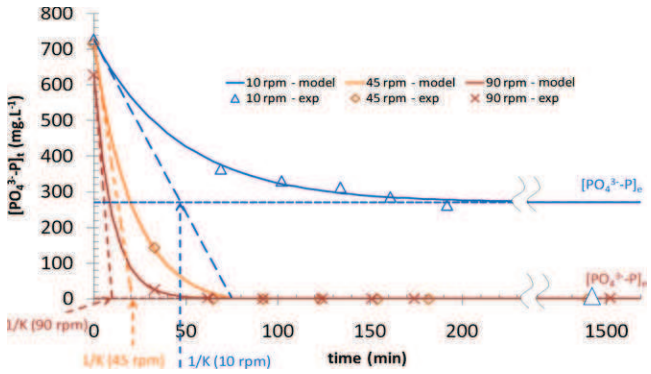

Fig. 1. The evolution of PO_4^{3-}-P follows a first order kinetic, temperature = 5 °C, initial Mg:Ca = 1.2–1.7, [Mg-MgO] = 800–1000 mg L^{-1}.

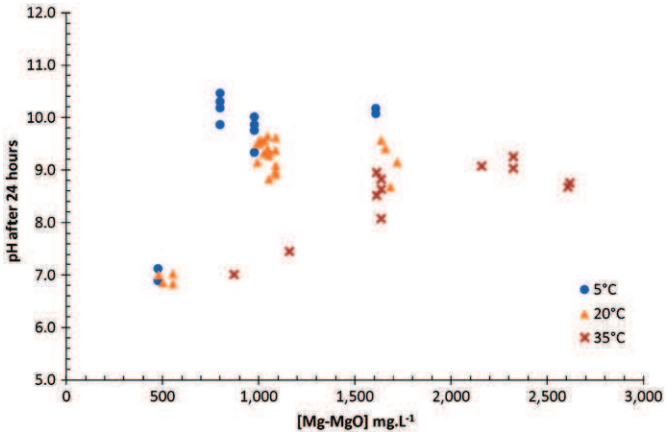

Fig. 3. The final pH is strongly related to [Mg-MgO] and to the temperature. pH reaches its maximum with 800 mg L^{-1} of [Mg-MgO] at 5 °C, with 1050 mg L^{-1} at 20 °C and with 1700 mg L^{-1} at 35 °C.

were below the limit calculated by the first order kinetic equation (Fig. 1, Δ). At 4 and 24 h, samples were collected for morphogranulometric characterization. The stirring rate was increased during 5 min in order to collect a homogeneous quote of particles. This stirring perturbed the results of the 10 rpm stirred runs. Therefore, the concentrations of the final PO_4-P were calculated thanks to the limit of (10) which equals to $[PO_4\text{-P}]_e$. $[PO_4\text{-P}]_e$ was then chosen to evaluate the influence of process parameters on P removal.

Over 48 runs, 44 were described by (10) (mean R^2 was 0.9998 and standard deviation was 2.47 mg L^{-1}). 4 runs were described by an affine function because the concentrations of PO_4-P at 30 min were below the quantification limit (10 mg L^{-1}) and more than two points are needed to evaluate $[PO_4\text{-P}]_e$. Therefore, the study was performed on the 44 runs described by (10).

After the addition of MgO in the beakers, the pH value increased from 4.5 to 7–8 in the first min. The pH values remained at 7–8 during 15–25 minutes. Afterward it increased from 7–8 to 9–10. For the runs at 5 °C, it remained constant until the end of the runs. For the runs at 20 °C and 35 °C, the pH decreased slightly by 0.5 to 1 unit after 12 h (Fig. 2). The temperature and the concentration of Mg^{2+} remaining as MgO ([Mg-MgO]) influenced the final pH values. Final pH was about 10–10.5 with 800 mg L^{-1} of [Mg-MgO] at 5 °C, about 9.5 with 1050 mg L^{-1} at 20 °C and about 9 with 1700 mg L^{-1} at 35 °C (Fig. 3). The final pH value depends on various phenomena, NH_3 volatilization, incorporation of carbonates, MgO dissolution. . ., which were dependent on the five process parameters studied.

Table 4
ANOVA for the final concentration of phosphates.

Process parameters	Prob. > F for $[PO_4\text{-P}]_e$
Adjusted R^2	66.28%
A:Stirring rate	0.0003 (−)
B:Temperature	0.2083 (−)
D:initial Mg^{2+}:Ca^{2+} molar ratio	0.2158 (−)
E: Mg^{2+} as MgO	0.0000 (−)
AA	0.0002 (+)
AB	0.0005 (+)
EE	0.0000 (+)

(+) indicates a positive influence and (−) a negative influence on the studied responses.

[Mg-MgO] and stirring rate were the leading process parameters which had a negative influence on $[PO_4\text{-P}]_e$ and consequently a positive influence on P removal (Table 4).

The interaction between the temperature and stirring rate was significant. Whatever the stirring rate, P was entirely removed at the end of the experiments at 35 °C, while $[PO_4\text{-P}]_e$ was up to 450 mg L^{-1} at 5 °C and a stirring rate of 10 rpm (Fig. 4).

When the stirring rate was at 10 rpm, the MgO settled and only the surface of MgO could react. The crystallization of struvite was lowered and the pH did not increase. This effect was partially counterbalanced by the increase of temperature that improved the diffusion and the dissolution of MgO in the medium. Therefore,

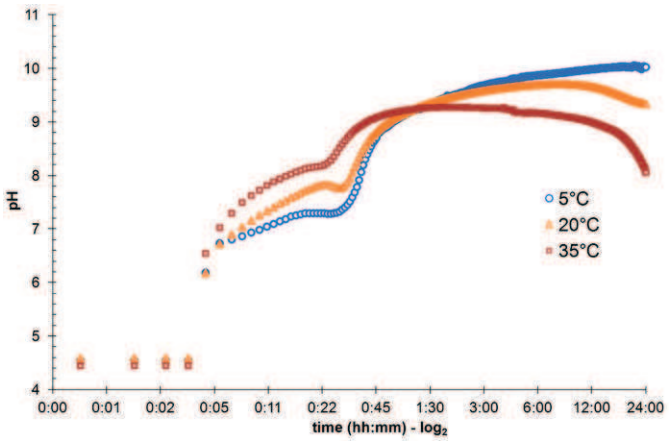

Fig. 2. The pH function of logarithm base 2 of the time evolved differently function of temperature – 5 °C run 10, 20 °C run 30, 35 °C run 42.

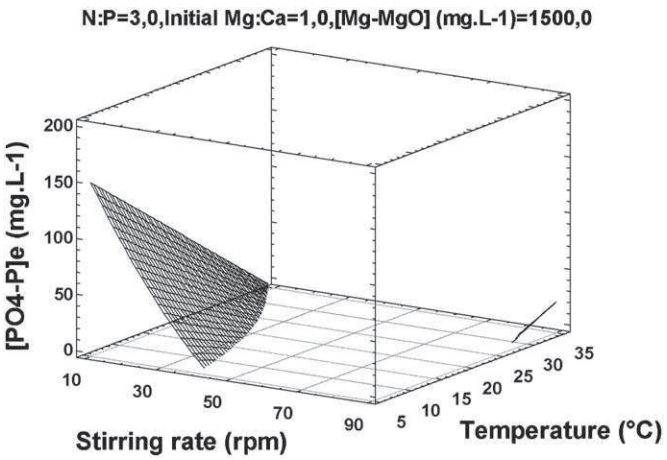

Fig. 4. Temperature and stirring rate negatively influence the final dissolved phosphate $[PO_4^{3-}\text{-P}]_e$, the grid represents the surface response of the statistical model.

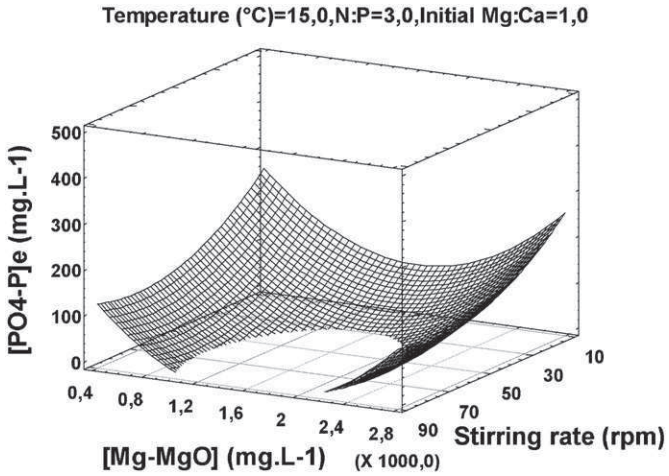

Fig. 5. [Mg-MgO] and stirring rate negatively influence the final dissolved phosphate $[PO_4^{3-}\text{-}P]_e$, the grid represents the surface response of the statistical model.

$[PO_4\text{-}P]_e$ remained high for the 10 rpm stirred runs (Fig. 5). The positive effect of the concentration of magnesium was also observed in literature with the addition of $Mg(OH)_2$ [25] or $MgCl_2$ plus NaOH [15].

3.1.2. Phosphate removal as struvite is mainly influenced by N:P ratio

P was supposed to form either struvite or calcium phosphate which was confirmed by Raman analysis (part 3.3.3). The percentage of phosphate as struvite is calculated according to (11) where M_N and M_P are the molecular mass of nitrogen and phosphorus respectively. $[NH_3\text{-}N]_{volatilized}$ is calculated using (12) in part 3.1.3.

$$\%PO_4 - P_{Struvite} = \frac{([NH_4 - N]_{initial} - [NH_4 - N]_{final} - [NH_3 - N]_{volatilized}) \times M_P}{M_N \times [PO_4 - P]_{initial}} \quad (11)$$

The ANOVA in Table 5 indicates that N:P molar ratio ($p<0.0001$) and temperature ($p<0.01$) were the leading process parameters that influenced the proportion of P as struvite.

$\%PO_4\text{-}P_{Struvite}$ increased from 20% to 90% with an increase in N:P molar ratio from 1 to 3. Abbona et al. [13] showed that a high Mg:Ca ratio (4:1) combined with a low pH (around 7) improved struvite formation over calcium phosphate formation. In this experimental design, the minimum Mg:Ca molar ratio was set at 2.25 to increase the pH value to at least 7. It appeared that above this ratio, the Mg:Ca molar ratio was not the limiting factor to struvite formation, it was the N:P molar ratio.

There are two possible explanations for the influence of the N:P molar ratio on the proportion of P as struvite. Firstly, NH_4^+ participates to struvite precipitation: the supersaturation increased with the N:P molar ratio and the nucleation rate of struvite was speeded up (1). Secondly, NH_4^+ improves the buffer capacity of the solution [18,35,36]. The nucleation of struvite occurs at a lower pH than the one needed for the precipitation of calcium phosphate [13]. Consequently, struvite precipitation is favoured by a high concentration of NH_4^+. However, as struvite precipitates, NH_4^+ buffering capacity decreases. Therefore, the effect of N:P molar ratio on the buffering capacity cannot be observed just by monitoring the pH.

Table 5
ANOVA for the proportion of P as struvite ($\%PO_4$-P as struvite).

Process parameters	Prob. > F for $\%PO_4$-P as struvite
Adjusted R^2	65.27%
B: Temperature	0.0089 (−)
C: N:P molar ratio	0.0000 (+)
BB	0.0740 (−)
BC	0.1000 (−)
CC	0.0472 (−)

(+) indicates a positive influence and (−) a negative influence on the studied responses.

Table 6
ANOVA for the percentage of ammonia volatilization.

Process parameters	Prob. > F for % NH_3 volatilization
Adjusted R^2	87.28%
B: Temperature	0.0006 (+)
E: Mg^{2+} as MgO	0.0000 (+)
BB	0.0005 (−)
BE	0.0004 (+)
EE	0.0002 (−)

(+) indicates a positive influence and (−) a negative influence on the studied responses.

$\%PO_4\text{-}P_{Struvite}$ decreased from 80% to 50% when temperature rose from 5 to 35 °C.

With high temperature, the pKa of NH_4^+/NH_3 decreases favouring the NH_3 form and NH_3 volatilization as described below. Therefore the supersaturation of struvite decreases and the phosphates are able to precipitate as calcium phosphate.

3.1.3. Ammonia volatilization is mainly influenced by temperature and addition of MgO

Molar balance for nitrogen highlighted a strong ammonia volatilization at the end of the runs. For each run, total ammonia volatilization was calculated using (12).

$$[NH_3 - N]_{volatilized} = [NH_4^+ - N]_{initial\ in\ liquid} - [NH_4^+ - N]_{final\ in\ liquid} - [NH_4^+ - N]_{final\ in\ solid} \quad (12)$$

[Mg-MgO] and temperature ($p<0.0001$) were the leading process parameters which influenced ammonia volatilization (Table 6).

The interaction between temperature and [Mg-MgO] was significant. Whatever concentration [Mg-MgO] had at 5 °C, NH_3 volatilization was below 10% at the end of the experiments, while the effect of [Mg-MgO] was high at high temperature (Fig. 6).

In literature, ammonia volatilization is function of pH, temperature and ammonium concentration [37]. In this experimental

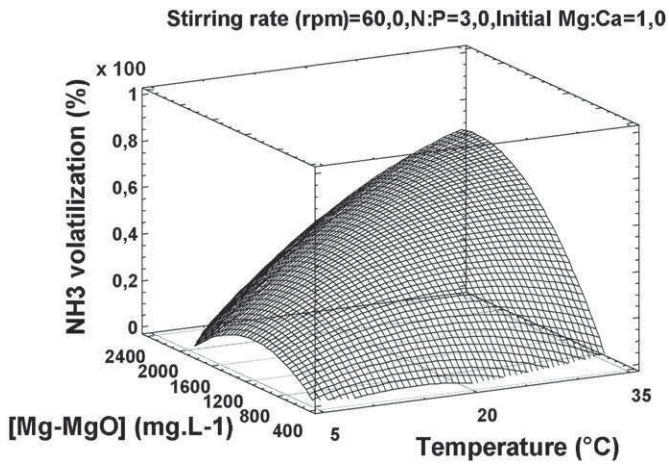

Fig. 6. [Mg-MgO] and temperature positively influence total NH_3 volatilization, the grid represents the surface response of the statistical model.

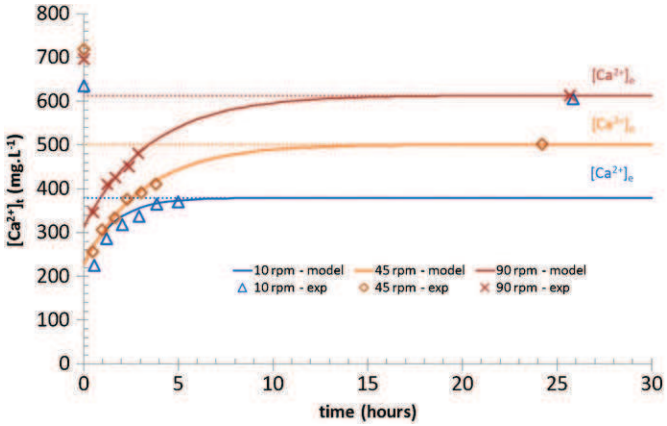

Fig. 7. Calcium apparent dissolution follows a first order kinetic, temperature = 20 °C, N:P = 3, initial Mg:Ca = 1.0–1.2, [Mg-MgO] = 1000–1600 mg L^{-1}.

design, initial N:P molar ratio and stirring rate had no significant influence on ammonia volatilization.

3.1.4. Phosphate precipitation as calcium phosphates is mainly influenced by stirring rate and N:P ratio

The calcium precipitation is very complex to explain as it could precipitate in several forms depending on the kinetic of struvite precipitation, pH, supersaturation, temperature...

Further solid analysis needs to be performed hourly to determine exactly the composition of the solid. In these experiments, a large part of the calcium was first removed within 30 min, and then, we observed an apparent dissolution of the removed calcium which followed a first order kinetic (Fig. 7 and (13)).

Over 48 runs, 43 were described by (13) (mean R^2 was 0.99 and standard deviation was 5.36 mg L^{-1}). 5 runs were excluded from the statistical analysis because there was no apparent dissolution of the calcium.

$$[Ca^{2+}]_t = ([Ca^{2+}]_e - [Ca^{2+}]_0) \times (1 - e^{-Kt}) + [Ca^{2+}]_0 \quad (13)$$

$[Ca^{2+}]_t$ and $[Ca^{2+}]_e$ are the concentration of the calcium totally dissolved at t and at equilibrium respectively. $[Ca^{2+}]_0$, the concentration when time equals 0 h, has no chemical reality. K is the kinetic constant of dissolution.

The N:P molar ratio and stirring rate were the leading parameters that influenced $[Ca^{2+}]_e$ (Table 7 and Fig. 8).

When stirring rate was below 10 rpm, precipitations or dissolutions of calcium phosphate and struvite and MgO were diffusion controlled [7,8]. Therefore, low stirring rates slowed down, or even prevented the dissolution of calcium phosphate.

Table 7A
ANOVA for the concentration of calcium at equilibrium.

Process parameters	Prob. > F for $[Ca^{2+}]_e$
Adjusted R^2	70.67%
A:Stirring rate	0.0003 (+)
B:Temperature	0.0152 (−)
C: N:P molar ratio	0.0000 (+)
D:initial Mg^{2+}:Ca^{2+} molar ratio	0.4254 (−)
E: Mg^{2+} as MgO	0.0093 (−)
AA	0.0006 (−)
BB	0.0000 (+)
BD	0.0075 (−)
CD	0.0171 (+)
DD	0.0115 (−)

(+) indicates a positive influence and (−) a negative influence on the studied responses.

Table 7B
ANOVA for particles >100 μm.

Process parameters	Prob. > F for particles > 100 μm (g/L)	Prob. > F for % particles > 100 μm
Adjusted R^2	69.43%	72.36%
A: Stirring rate		0.3431 (+)
B: Temperature	0.0062 (−)	0.0460 (−)
C: N:P molar ratio	0.0029 (+)	0.0361 (+)
E: Mg^{2+} as MgO	0.0000 (−)	0.0000 (−)
AE		0.0474 (−)
EE	0.0000 (+)	0.0000 (+)

(+) indicates a positive influence and (−) a negative influence on the studied responses.

The influence of N:P molar ratio on $[Ca^{2+}]_e$ confirms the previous results: high N:P molar ratio improved struvite precipitation instead of calcium phosphate precipitation.

3.2. Influence of process parameters on dried products

The three solid fractions (<25 μm, 25–100 μm and >100 μm) were weighed and analyzed by ion chromatography after acid dissolution and by Raman spectroscopy.

In order to assess mass balance in dried solids, phosphates are considered as struvite and ACP (part 3.3), calcium was thought to precipitate as ACP and $CaCO_3$ and magnesium was considered as MgO and struvite (14). As runs were all carried out in an open beaker, carbonate was either incorporated to the crystals or precipitated as calcite [38]. The linear formula used for ACP was $Ca_2P_2O_7{\cdot}H_2O$.

$$m_{\text{dried solid}} = m_{MgO} + m_{\text{Struvite}} + m_{ACP} + m_{CaCO_3} + m_{Na^+} + m_{K^+} + m_{Cl^-} + m_{NO_2^-} + m_{NO_3^-} + m_{SO_4^{2-}} \quad (14)$$

For 80% of the runs, the absolute error on mass balance was below the sum of experimental errors (20%). These results confirmed the hypothesis that calcium could precipitate as ACP and as calcium carbonate. The absolute error on mass balance was significant in a third of the fine particles and in a fifth of the particles >100 μm obtained at 35 °C. The Raman analyses (3.3.3) show that magnesium precipitated as $Mg(OH)_2$ (brucite) instead of remaining as MgO in small particles or instead of $CaCO_3$ in large particles.

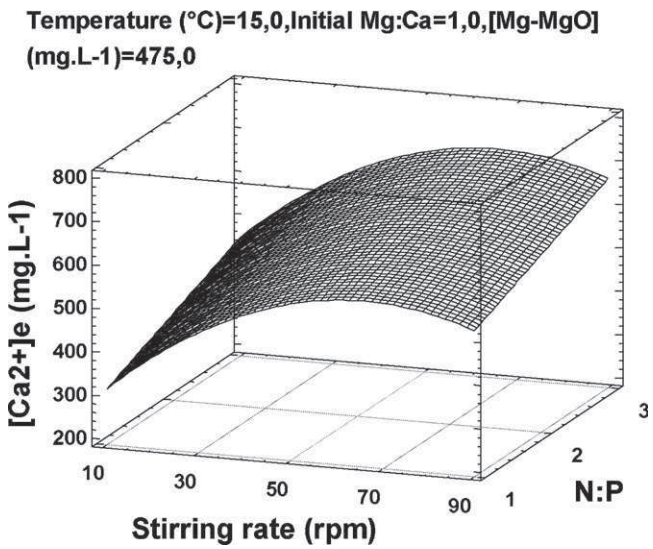

Fig. 8. Stirring rate and N:P molar ratio positively influence $[Ca^{2+}]_e$, the grid represents the surface response of the statistical model.

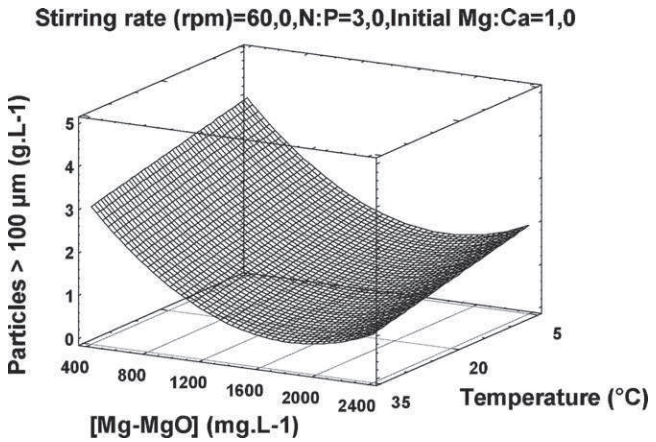

Fig. 9. [Mg-MgO] and temperature negatively influence concentration of particles bigger than 100 μm, the grid represents the surface response of the statistical model.

3.2.1. Particles >100 μm are mainly influenced by the addition of MgO

The influence of process parameters was studied on the fractions >100 μm; the filtration of struvite crystals are carried out in filter bags with a 100 μm cut-off in the process plant. The ANOVA in Table 7 indicated that [Mg-MgO] ($p<0.0001$), temperature and N:P molar ratio were the leading process parameters which influenced the particles >100 μm (Fig. 9).

The struvite growth is assumed to be size dependent [11]: small nuclei produce small crystals ultimately. Moreover, the higher the supersaturation (β) is, the smaller nuclei are [5,7,8]. Therefore, as high concentrations of Mg^{2+} increase the supersaturation of struvite, the quantity of fine crystals is increased too. The influence of [Mg-MgO] on the struvite growth is very complex. [Mg-MgO] influenced the pH (and so the phosphate removal), the concentration of Mg^{2+} (and so the supersaturation), the crystallization as nucleation of struvite could occur on the particles of MgO... Further studies are needed to better understand the influence of this parameter on the kinetics.

When temperature rises, the supersaturation of struvite decreases, so the size of the crystals increases [39]. This assertion is true only when NH_4^+ is not a limiting factor in struvite crystallization. Otherwise, as temperature increases, Henry's law constant (K_H) and dissociation constant (K_a) of ammonia evolve to favour greater NH_3/NH_4^+ ratio in liquid and ammonia volatilization [37]. Therefore, when dissolved NH_4^+ is a limiting factor, NH_3 volatilization will slow down struvite crystallization and struvite crystals will dissolve in order to restore the balance to NH_4^+ in the solution. On this account, the temperature has a negative impact on crystal sizes.

The effect of stirring is to maintain MgO in suspension (interaction AE). Without it, the pH will not rise to the minimal value for P precipitation. However, high mixing rates have a negative impact on struvite crystal sizes. Two mechanisms could be involved: struvite dissolution or crystal break. As the full amount of struvite did not change, breaking was more probable.

3.2.2. The proportion of struvite versus calcium phosphate is mainly influenced by particles size and N:P ratio

The experimental design in Statgraphics software was modified to include the influence of particles size (<25 μm, 25 - 100 μm or >100 μm) on the proportion of struvite versus calcium phosphate. R^2 of statistical model in Table 8 was below 65% so it was said to only indicate trends.

The ANOVA in Table 8 indicated that particle size ($p<0.0001$), N:P molar ratio ($p<0.001$) and temperature ($p<0.05$) were the leading process parameters which influenced the proportion of struvite versus calcium phosphate in dried solids (%).

Table 8
ANOVA for proportion of struvite versus calcium phosphate in dried solid (%).

Process parameters	Prob. > F for proportion of struvite versus calcium phosphate in dried solid (%)
Adjusted R^2	62.78%
B: N:P	0.0004 (+)
D: [Mg-MgO]	0.2961 (−)
E: Temperature	0.0177 (−)
F: Particle size	0.0000 (+)
BE	0.0495 (+)
DD	0.0477 (+)
FF	0.0000 (−)

(+) indicates a positive influence and (−) a negative influence on the studied responses.

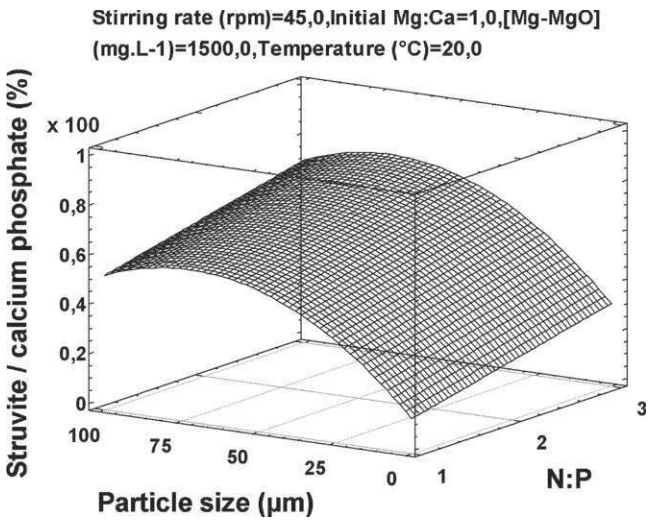

Fig. 10. Particle size and N:P molar ratio positively influence the proportion of struvite versus calcium phosphate in dried solid, the grid represents the surface response of the statistical model.

Struvite was the main component of the fractions >25 μm for all level of variables (Fig. 10).

The influence of N:P molar ratios on the proportion of struvite versus calcium phosphate confirms the results of the previous part: with a high N:P molar ratio, struvite precipitation was favoured over calcium phosphate precipitation.

3.3. Analyses of the solid fractions

3.3.1. Potential solid phases with PHREEQC®

The potential final precipitates are defined by a SI > 0.5; the SI values for the 48 runs are given in Table 10. ACP, calcite and struvite could precipitate in all the runs. Brucite, brushite, calcium and magnesium phosphate could precipitate in most of the runs as shown in Table 11. Hydromagnesite and artinite could precipitate, but, in literature, there were either not observed in association with struvite precipitation or they could only biomineralize with the help of bacteria [40,41].

3.3.2. Calcium phosphate precipitates as ACP

The forms of calcium phosphate precipitated were determined by calculating the Ca:P molar ratio in the three solid fractions using (15):

$$Ca:P = \frac{Ca_{Precipitated}}{P_{Precipitated} - N_{Precipitated}} \quad (15)$$

Table 10A
SI values for the potential precipitates after 24 h for the 48 runs.

Minerals	Formula	Min	Max	Median	Nb run SI>0.5
pH		6.84	10.47	9.20	
Temperature (°C)		5.00	35.00	20.00	
Artinite	$MgCO_3{\cdot}Mg(OH)_2{\cdot}3H_2O$	-7.12	3.18	1.64	36
Brucite	$Mg(OH)_2$	-0.84	6.51	5.26	42
Brushite (DCPD)	$CaHPO_4{\cdot}2H_2O$	0.12	1.00	0.58	38
Calcium phosphate	$CaHPO_4$	0.40	1.36	0.80	46
Calcite	$CaCO_3$	0.63	3.09	2.76	48
Calcite hydrate	$CaCO_3{\cdot}H_2O$	−0.71	1.75	1.42	40
Hydromagnesite	$Mg_5(CO_3)_4(OH)_2{\cdot}4H_2O$	−12.62	8.83	4.71	40
K-Struvite	$MgKPO_4{\cdot}6H_2O$	−2.09	1.06	0.47	26
Magnesium phosphate	$Mg_3(PO_4)_2$	−1.28	5.29	4.03	41
Newberyite	$MgHPO_4{\cdot}3H_2O$	−0.33	0.64	0.26	10
Struvite	$MgNH_4PO_4{\cdot}6H_2O$	0.47	3.07	2.52	48
ACP	$Ca_3(PO_4)_2{\cdot}xH_2O$	1.33	6.74	5.42	48

Table 10B
Ca:P molar ratio in various calcium phosphates precipitates [45].

Ca:P molar ratio	Name	Formula	pH stability range in aqueous solutions at 25 °C
1.00	Brushite	$CaHPO_4{\cdot}2H_2O$	2.0–6.0
1.33	Octacalcium phosphate	$Ca_8(HPO_4)_2(PO_4)_4{\cdot}5H_2O$	5.5–7.0
1.00–2.20	ACP	$Ca_xH_y(PO_4)_z{\cdot}nH_2O$	5.0–12.0
1.50–1.67	Calcium-deficient hydroxyapatite	$Ca_{10-x}(HPO_4)_x(PO_4)_{6-x}(OH)_{2-x}$	6.5–9.5
1.67	Hydroxyapatite	$Ca_{10}(PO_4)_6(OH)_2$	9.5–12.0

Where $Ca_{Precipitated}$, $P_{Precipitated}$ and $N_{Precipitated}$ are the calcium, phosphorus and nitrogen precipitated in $mol.g^{-1}$ of solidrespectively. Nitrogen is assumed to only precipitate as struvite.

In the fractions < 25 μm, Ca:P molar ratio was near 0.90 which indicates the possible presence of brushite or ACP (Table 10). The form of calcium phosphate was probably ACP as the minimum pH values of the runs were higher than 6.0. The literature confirms the result that ACP co-precipitates with struvite [14,19,21,42,43]. The incorporation of Mg^{2+} into the structure of ACP could explained why the Ca:P molar ratio was inferior to 1 and why ACP particles were mainly in the fraction < 25 μm [12,32].

In the fractions >25 μm, Ca:P molar ratios were below 0.7. Calcium might be incorporated in struvite structure.

Ca:P molar ratio was higher than 1.2 for the majority of the fractions >100 μm and obtained at 35 °C. Raman spectrum for these fractions showed the characteristic peaks of $CaCO_3$ (Fig. 11, part 3.3.3). Moreover, the Fig. 2 in part 3.1.1 shows that the pH values decreased after 12 h in the runs at 35 °C. The precipitation of $CaCO_3$ could explain this decrease [44].

3.3.3. Solid analyses by Raman spectroscopy

Calcite, calcium phosphate, HAP, $MgCO_3$, magnesium phosphate, newberyite, brucite, MgO, ammonium phosphate and struvite (analytic grade) were analyzed by Raman spectroscopy to have reference spectra.

The Raman spectrum for struvite showed two main peaks for phosphate vibrations, one at $950cm^{-1}$ (total symmetric stretching mode of $-PO_4$) and one at $565cm^{-1}$ (ν_4 antisymmetric bend mode of $-PO_4$) and two peaks corresponding to ammonium vibrations, one at $1440cm^{-1}$ (ν_4 mode of $-NH_4$) and one at $1700cm^{-1}$ (ν_2 mode of $-NH_4$) (spectrum (f) in Fig. 11). These Raman shifts are in line with literature results [38,46–48].

Presence, absence and height ratio of these four peaks indicate whether the product mainly contains struvite or not.

The Raman spectrum for brucite showed 3 characteristic peaks: 3 strong bands at 278, 443 (symmetric E_g and A_{1g} stretching mode) and $1085cm^{-1}$ and one broad peak at $1044cm^{-1}$ which is coherent with literature [49].

The Raman spectra of the solid fractions confirmed the results of Table 10. ACP, struvite and brucite were the main component of the fractions < 25 μm (spectrum (a) in Fig. 11 and in Table 11).

At 5 and 20 °C, struvite was the main component of the fractions >25 μm (spectra (d) and (e) in Fig. 11 and in Table 11). At 20 °C, the composition of the fractions >100 μm depended on other process parameters rather than on particles size or temperature (spectra (c) in Fig. 11).

At 35 °C the main compound was not struvite which was in line with solid dissolution analysis.

It is noticeable that the spectrum at 5 °C for fine particles (a) was similar to the spectrum at 35 °C for particles >100 μm (b). Those spectra presented three characteristic peaks of carbonate precipitation: one at $1080cm^{-1}$ (ν_1 symmetric stretch mode of $-CO_3$), a broad one at $715cm^{-1}$ (ν_2 mode of $-CO_3$) [50] and one at $2906cm^{-1}$ (could be attributed to $CaCO_3$). Compared to struvite spectrum, peaks at $435cm^{-1}$ (ν_2 symmetric bend mode of $-PO_4$) shifted by $+15cm^{-1}$ which could indicate the presence of calcium phosphate [51]. The feature peaks at 278, and $442cm^{-1}$ could also indicate the presence of brucite [49]. The main peak at $945cm^{-1}$ either was very low or had vanished. Moreover, two peaks appeared one at $1050cm^{-1}$ (ν_3 antisymmetric stretch mode

Table 11
Struvite is the main component of particles > 25 μm obtained at 5 and 20 °C.

Temperature (°C)	5 °C			20 °C			35 °C		
Particles size (μm)	<25	25–100	>100	<25	25–100	>100	<25	25–100	>100
Composition	ACP = MAP* > Br* > Calcite	MAP > CaP* = Br	MAP > Br	MAP > ACP > Br	MAP > Br	MAP > Br	Br > ACP > MAP	Br = MAP > ACP	Br > ACP > MAP

*MAP: struvite, Br: Brucite, CaP: Calcium phosphate, =: same proportion, >: higher proportion.

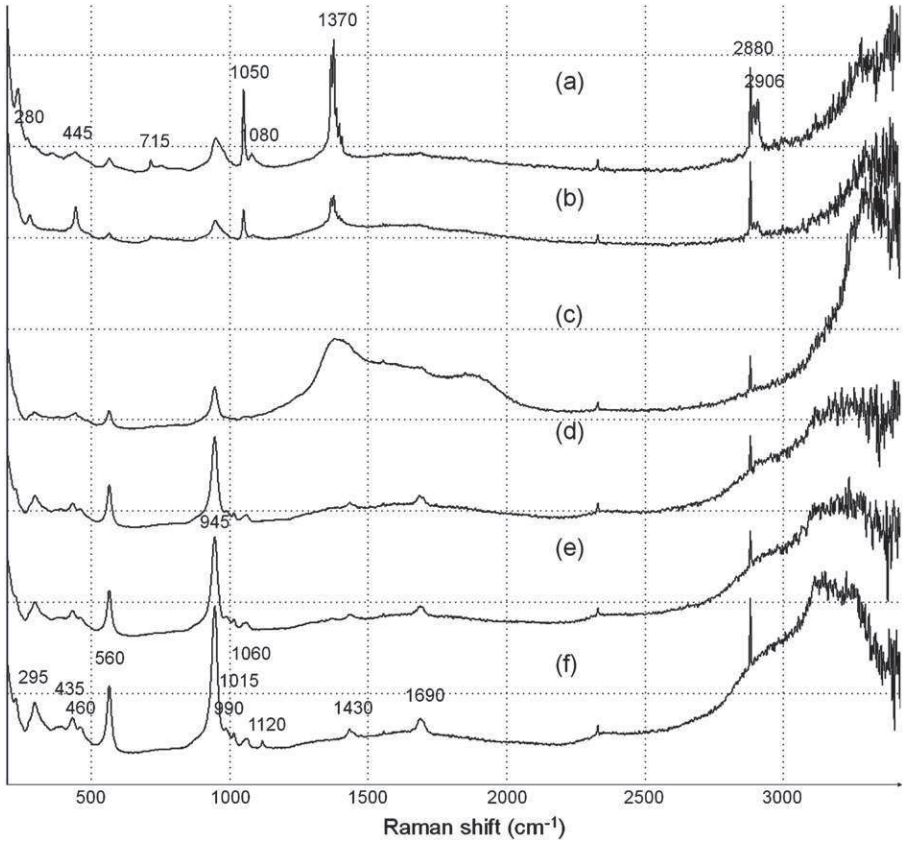

Fig. 11. Raman shift spectra of particles < 25 μm (a) and >100 μm (b) to (e) function of temperature: the runs 3 and 12 at 5 °C (a) and the runs 42 and 47 at 35 °C (b) may contain ACP, brucite and calcite, the runs 28 at 20 °C (c) may contain struvite and brucite, the run 29 at 20 °C (d) and the run 2 at 5 °C (e) may contain only struvite. (f) is pure struvite from Carlo Erba (99%)Optimization of process parameters for maximizing struvite precipitation.

Table 12
Process parameters levels for optimal desirability.

Process parameters	Levels	Levels at 15 °C and 60 rpm
A:Stirring rate	80 rpm	60 rpm
B:Temperature	5 °C	15.0 °C
C:N:P molar ratio	3	3
D:initial Mg^{2+}:Ca^{2+} molar ratio	0.6	1.7
E: Mg^{2+} as MgO	520 mg L^{-1}	500 mg L^{-1}

of –PO_4) and another at 1370cm^{-1}. Spectra (a) and (b) showed the presence of the characteristic peaks of phosphate, carbonate and brucite. Calcium carbonate, brucite and calcium phosphate could have precipitated in these fractions. The precipitation of $CaCO_3$ has been already observed in struvite precipitation processes [15,52].

The optimization aimed to minimize $[PO_4^{3-}\text{-P}]_e$ and ammonia volatilization, and maximize the production of big particles of struvite. The optimum levels of parameters are given in Table 12.

A low temperature is difficult to apply in an on-farm processing plant. The process plant could stay in a closed room but temperature variations cannot be avoided. Therefore, the optimal response for the design experiment was estimated at 15 °C, the annual average temperature in Brittany (Table 12 and Table 13). Stirring rate was lowered at 60 rpm, compared to the optimal 80 rpm, due to facility restrictions.

The multiple response optimization problems were solved by combining the responses into a single index: the desirability function.

[Mg-MgO] was the leading variable that influenced the precipitation of struvite (Fig. 12). When [Mg-MgO] was low, small variations of temperature, stirring rate or initial Mg:Ca did not affect the desirability which stayed in a range of 0.8–1. However, variations of the N:P molar ratio affected the desirability which decreased to 0.6 for a N:P molar ratio of 1.

In literature, the optimal pH for the struvite precipitation is in a range 8 to 10 [22,24,53]. We showed that after 24 h, in "swine wastewater conditions", the optimal pH was near 7. The Fig. 3

Table 13
Predicted and experimental responses for optimal desirability.

Responses	Weight	Impact	Optimal predicted response	Predicted response at 15 °C and 60 rpm	Experimental response at 15 °C and 60 rpm
Desirability		3	0.90	0.86	
$[PO_4\text{-P}]_e$	1	3	80 mg L^{-1}	60 mg L^{-1}	43 ± 12 mg L^{-1}
Particles >100 μm	1	3	3.6 g L^{-1}	3.4 g L^{-1}	3.5 ± 0.3 g L^{-1}
% particles > 100 μm	1	3	67%	60%	87 ± 1%
% PO_4-P as struvite	1	3	100%	96%	97 ± 3%
% ammonia volatilization	1	3	2%	8%	1 ± 1%

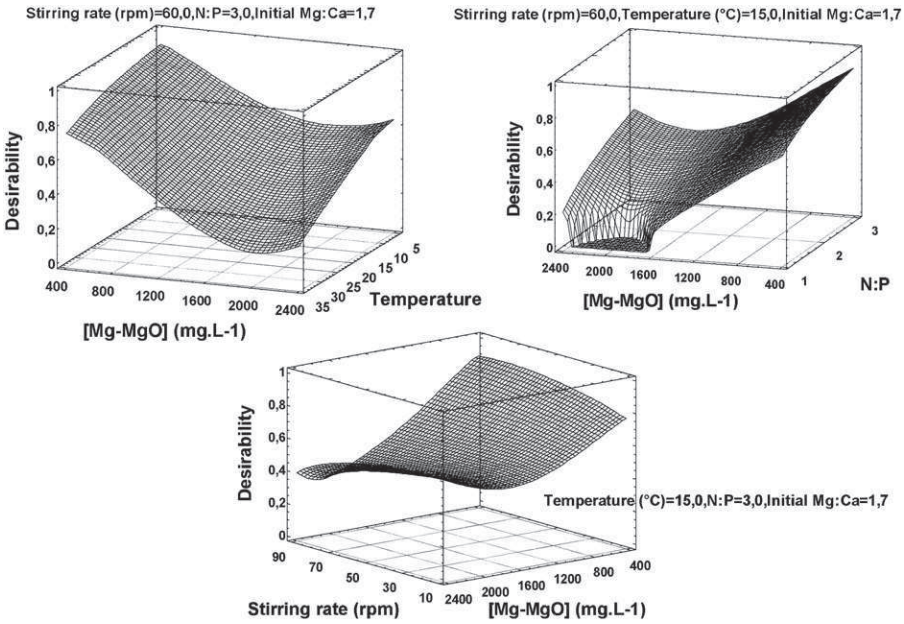

Fig. 12. [Mg-MgO] is the leading variable that influences the statistical responses of the design of experiments.

shows that this pH value corresponded to about 500 mg L^{-1} of [Mg-MgO]. This is coherent with a study of Battistoni et al. which said that the presence of calcium speeds up the struvite precipitation at lower pH values [54].

3.4. Precipitation with the optimized levels for variables

The precipitation of struvite was performed again with the best conditions. The experiments were triplicated. One more experiment was performed to monitor the ammonia volatilization. The N:P molar ratio was 3.2 and the Mg:Ca molar ratio was 2.3. Maximal pH was then 6.7. The experimental responses are presented in Table 13.

After 24 h, all particles were in the fractions >25 μm. The MgO entirely dissolved and the particles of calcium phosphate were in the fractions >25 μm.

The proportion of struvite versus calcium phosphate in dried solids was 76% ± 9% in the fraction 25 - 100 μm and increased to

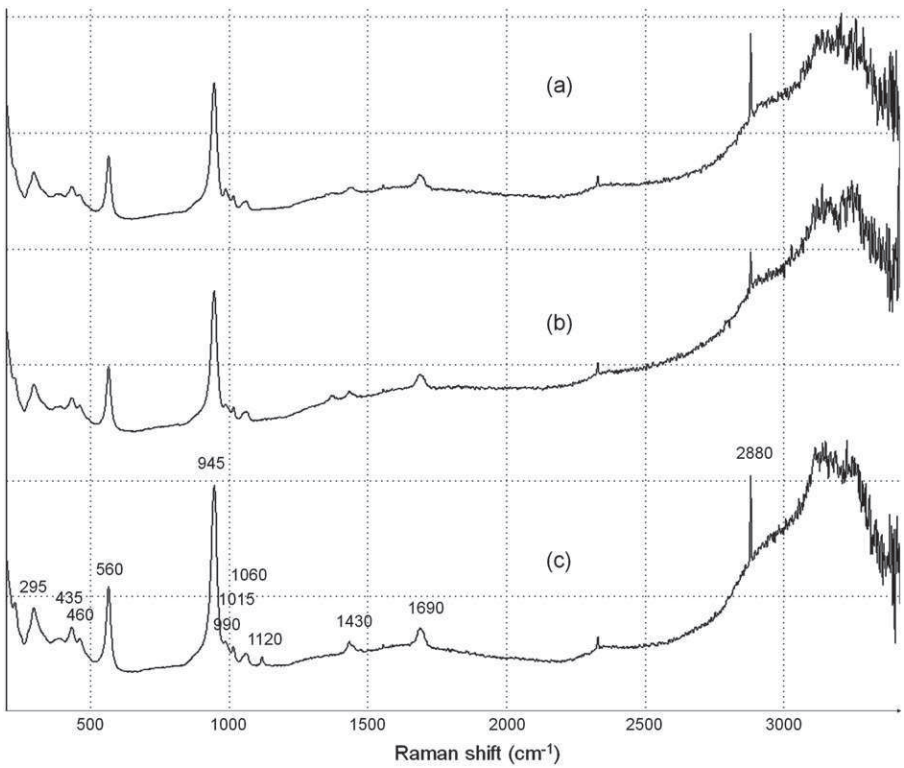

Fig. 13. Raman shift spectra of particles sieved after 24 h at 15 °C suggest that struvite is the main component: of particles bigger than 100 μm (a) and of particles between 25 and 100 μm (b). (c) is pure struvite from Carlo Erba (99%).

86% ± 2% in the fraction >100 μm. These results confirm the results of the statistical model.

The optimal levels for variables might have not only improved the size of struvite crystals but also increased the size of calcium phosphate particles. In part 3.3, a Ca:P molar ratio near 1 indicated the presence of ACP. In the 48 runs, this ratio was observed in the fractions < 25 μm. In the optimization run, this ratio was observed in the fraction 25 - 100 μm. ACP could have precipitated in this solid fraction. However Raman analysis (spectrum (b) in Fig. 13) did not show the characteristic peaks of calcium phosphate: the proportion of struvite in dried solids was much larger than calcium phosphate.

In the optimization run, Ca:P molar ratio was 0.57 ± 0.04 in the fraction >100 μm which was similar to results obtained in experimental design.

4. Conclusions

The optimization of the precipitation of struvite in a stirred beaker made it possible to recycle more than 90% of phosphorus in large crystals of struvite despite of the presence of large amounts of calcium and using a cheap reactant such as MgO.

The optimal conditions for the removal of phosphorus as large crystals of struvite in synthetic swine wastewater were: low Mg:Ca molar ratio (2.25:1), the leading parameter, high N:P molar ratio (3:1), moderate stirring rate (between 45 and 90 rpm) and low temperature (below 20 °C).

High N:P molar ratio improved the precipitation of struvite instead of calcium phosphate. Low concentrations of MgO induced a low supersaturation which improved the size of the struvite crystals; it also minimized ammonia volatilization.

Raman analysis and solid dissolution in acid made the identification of the composition of the product possible. These analyses revealed that: ACP co-precipitated with struvite, carbonates were incorporated into solid fractions and brucite precipitated in almost all of the runs. The Raman analyses were coherent with the SI values calculated by Phreeqc.

The runs lasted for 24 h in order to reach equilibrium. The size and the composition of the precipitated solids could evolve before reaching the equilibrium. Further analysis is needed to understand evolution of the solid phases over 24-hours.

Acknowledgements

This work is supported by the "Conseil Régional de la Bretagne", by the French Research National Agency (ANR) and by specific university research (MSMT No 21/2012).

References

[1] A. Smit, P. Bindraban, J. Schröder, J. Conjin, H. Van der Meer, Phosphorus in Agriculture: Global Resources, Trends and Developments, Report to the Steering Committee Technology Assessment of the Ministry of Agriculture, The Neetherlands, Wageningen, 2009.
[2] R. Gonzalez Ponce, Evaluation of struvite as a fertilizer: a comparison with traditional P sources, Agrochimica 51 (2007) 301–308.
[3] M.-L. Daumer, F. Béline, M. Spérandio, C. Morel, Relevance of a perchloric acid extraction scheme to determine mineral and organic phosphorus in swine slurry, Bioresour. Technol. 99 (2008) 1319–1324.
[4] M.-L. Daumer, S. Picard, P. Saint-Cast, P. Dabert, Technical and economical assessment of formic acid to recycle phosphorus from pig slurry by a combined acidification-precipitation process, J. Hazard. Mater. 180 (2010) 361–365.
[5] K.S. Le Corre, Understanding Struvite Crystallisation and Recovery, Cranfiel University, School of Applied Science, Department of Sustainable System, Center for Water Science, 2006.
[6] N. Hutnik, K. Piotrowski, B. Wierzbowska, A. Matynia, Continuous reaction crystallization of struvite from phosphate(V) solutions containing calcium ions, Cryst. Res. Technol. 46 (2011) 443–449.
[7] J. Mullin, Crystallization, fourth ed., Butterworth Heinemann, 2001.
[8] A. Mersmann, Crystallization Technology Handbook, second, CRC, 2001.
[9] M.I.H. Bhuiyan, D.S. Mavinic, R.D. Beckie, Nucleation and growth kinetics of struvite in a fluidized bed reactor, J. Cryst. Growth 310 (2008) 1187–1194.
[10] K. Byrappa, International School on Crystal Growth of Technologically Important Electronic Materials, Allied Publishers, 2003.
[11] J. Koralewska, K. Piotrowski, B. Wierzbowska, A. Matynia, Kinetics of reaction-crystallization of struvite in the continuous draft tube magma type crystallizers—influence of different internal hydrodynamics, Chin. J. Chem. Eng. 17 (2009) 330–339.
[12] F. Abbona, M. Franchini-Angela, Crystallization of calcium and magnesium phosphates from solutions of low concentration, J. Cryst. Growth 104 (1990) 661–671.
[13] F. Abbona, H.E.L. Madsen, R. Boistelle, The initial phases of calcium and magnesium phosphates precipitated from solutions of high to medium concentrations, J. Cryst. Growth 74 (1986) 581–590.
[14] F. Abbona, H.E. Lundager Madsen, R. Boistelle, The final phases of calcium and magnesium phosphates precipitated from solutions of high to medium concentration, J. Cryst. Growth 89 (1988) 592–602.
[15] I. Kabdaşli, O. Tünay, M.Ş. Çetin, T. Ölmez, Assessment of magnesium ammonium phosphate precipitation for the treatment of leather tanning industry wastewaters, Water Sci. Technol. 46 (2002).
[16] O. Tünay, I. Kabdasli, D. Orhon, S. Kolçak, Ammonia removal by magnesium ammonium phosphate precipitation in industrial wastewaters, Water Sci. Technol. 36 (1997) 225–228.
[17] M.L. Daumer, F. Béline, S.A. Parsons, Chemical recycling of phosphorus from piggery wastewater, in: Intl Water Assn, Vancouver, 2009, pp. 339–350.
[18] I. Lopez-Valero, C. Gomez-Lorente, R. Boistelle, Effects of sodium and ammonium ions on occurrence, evolution and crystallinity of calcium phosphates, J. Cryst. Growth 121 (1992) 297–304.
[19] D. Crutchik, J.M. Garrido, Struvite crystallization versus amorphous magnesium and calcium phosphate precipitation during the treatment of a saline industrial wastewater, Water Sci. Technol. 64 (2011) 2460.
[20] K.S. Le Corre, E. Valsami-Jones, P. Hobbs, S.A. Parsons, Kinetics of struvite precipitation: effect of the magnesium dose on induction times and precipitation rates, Environ. Technol. 28 (2007) 1317–1324.
[21] Z.-L. Ye, S.-H. Chen, S.-M. Wang, L.-F. Lin, Y.-J. Yan, Z.-J. Zhang, et al., Phosphorus recovery from synthetic swine wastewater by chemical precipitation using response surface methodology, J. Hazard. Mater. 176 (2010) 1083–1088.
[22] J.D. Doyle, R. Philp, J. Churchley, S.A. Parsons, Analysis of struvite precipitation in real and synthetic liquors, Process Saf. Environ. Prot. 78 (2000) 480–488.
[23] A. Uysal, Y.D. Yilmazel, G.N. Demirer, The determination of fertilizer quality of the formed struvite from effluent of a sewage sludge anaerobic digester, J. Hazard. Mater. 181 (2010) 248–254.
[24] D. Kim, H.-D. Ryu, M.-S. Kim, J. Kim, S.-I. Lee, Enhancing struvite precipitation potential for ammonia nitrogen removal in municipal landfill leachate, J. Hazard. Mater. 146 (2007) 81–85.
[25] E.V. Münch, K. Barr, Controlled struvite crystallisation for removing phosphorus from anaerobic digester sidestreams, Water Res. 35 (2001) 151–159.
[26] J. Goupy, Les plans d'expérience pour surface de réponse, Dunod, 1999.
[27] M. Hanhoun, L. Montastruc, C. Azzaro-Pantel, B. Biscans, M. Frèche, L. Pibouleau, Temperature impact assessment on struvite solubility product: a thermodynamic modeling approach, Chem. Eng. J. 167 (2011) 50–58.
[28] A. Mañas, M. Pocquet, B. Biscans, M. Sperandio, Parameters influencing calcium phosphate precipitation in granular sludge sequencing batch reactor, Chem. Eng. Sci. 77 (2012) 165–175.
[29] M. Altmaier, V. Metz, V. Neck, R. Müller, T. Fanghänel, Solid-liquid equilibria of Mg(OH)2(cr) and Mg2(OH)3Cl 4H2O(cr) in the system Mg-Na-H-OH-Cl-H2O at 25 °C, Geochim. Cosmochim. Acta 67 (2003) 3595–3601.
[30] J.C. Deelman, Low-Temperature Formation of Dolomite and Magnesite, Compact Disc Publications, 2003.
[31] X.L. Deng, Y.M. Luo, M.M. Xu, X.Y. Hu, Influence of solvent polarity on synthesis of beta – tricalcium phosphate, Key Eng. Mater. 330–332 (2007) 143–146.
[32] F. Abbona, A. Baronnet, A XRD and TEM study on the transformation of amorphous calcium phosphate in the presence of magnesium, J. Cryst. Growth 165 (1996) 98–105.
[33] P. Battistoni, A. De Angelis, P. Pavan, M. Prisciandaro, F. Cecchi, Phosphorus removal from a real anaerobic supernatant by struvite crystallization, Water Res. 35 (2001) 2167–2178.
[34] M. Quintana, E. Sanchez, M.F. Colmenarejo, J. Barrera, G. Garcia, R. Borja, Kinetics of phosphorus removal and struvite formation by the utilization of by-product of magnesium oxide production, Chem. Eng. J. 111 (2005) 45–52.
[35] A.A. Szögi, M.B. Vanotti, Removal of phosphorus from livestock effluents, J. Environ. Qual. 38 (2009) 576.
[36] M.B. Vanotti, A.A. Szogi, P. Hunt, Extraction of soluble phosphorus from swine wastewater, Trans. ASAE 46 (2003) 1665–1674.
[37] F. Montes, C.A. Rotz, H. Chaoui, Process modeling of ammonia volatilization from ammonium solution and manure surfaces: a review with recommended models, Trans. ASABE 52 (2009) 1707–1719.
[38] M. Kazanci, P. Fratzl, K. Klaushofer, E.P. Paschalis, Complementary information on in vitro conversion of amorphous (precursor) calcium phosphate to hydroxyapatite from raman microspectroscopy and wide-angle X-ray scattering, Calcif. Tissue Int. 79 (2006) 354–359.
[39] M. Ronteltap, M. Maurer, R. Hausherr, W. Gujer, Struvite precipitation from urine – influencing factors on particle size, Water Res. 44 (2010) 2038–2046.
[40] M. Rivadeneyra, R. Delgado, J. Párraga, A. Ramos-Cormenzana, G. Delgado, Precipitation of minerals by 22 species of moderately halophilic bacteria in artificial marine salts media: Influence of salt concentration, Folia Microbiol. 51 (2006) 445–453.

[41] M. Sánchez-Román, C.S. Romanek, D.C. Fernández-Remolar, A. Sánchez-Navas, J.A. McKenzie, R.A. Pibernat, et al., Aerobic biomineralization of Mg-rich carbonates: Implications for natural environments, Chem. Geol. 281 (2011) 143–150.
[42] L. Pastor, D. Mangin, J. Ferrer, A. Seco, Struvite formation from the supernatants of an anaerobic digestion pilot plant, Bioresour. Technol. 101 (2010) 118–125.
[43] N. Martí, L. Pastor, A. Bouzas, J. Ferrer, A. Seco, Phosphorus recovery by struvite crystallization in WWTPs: Influence of the sludge treatment line operation, Water Res. 44 (2010) 2371–2379.
[44] J.A. Wojtowicz, Calcium carbonate precipitation potential, J. Swimming Pool Spa Ind. 2 (2001) 23–29.
[45] S.V. Dorozhkin, Amorphous calcium (ortho)phosphates, Acta Biomater. 6 (2010) 4457–4475.
[46] R.L. Frost, M.L. Weier, W.N. Martens, D.A. Henry, S.J. Mills, Raman spectroscopy of newberyite, hannayite and struvite, Spectrochim. Acta A 62 (2005) 181–188.
[47] V. Stefov, B. Šoptrajanov, I. Kuzmanovski, H.D. Lutz, B. Engelen, Infrared and Raman spectra of magnesium ammonium phosphate hexahydrate (struvite) and its isomorphous analogues. III. Spectra of protiated and partially deuterated magnesium ammonium phosphate hexahydrate, J. Mol. Struct. 752 (2005) 60–67.
[48] V. Stefov, B. Šoptrajanov, F. Spirovski, I. Kuzmanovski, H. Lutz, B. Engelen, Infrared and Raman spectra of magnesium ammonium phosphate hexahydrate (struvite) and its isomorphous analogues. I. Spectra of protiated and partially deuterated magnesium potassium phosphate hexahydrate, J. Mol. Struct. 689 (2004) 1–10.
[49] F. Pascale, S. Tosoni, C. Zicovich-Wilson, P. Ugliengo, R. Orlando, R. Dovesi, Vibrational spectrum of brucite, $Mg(OH)_2$: a periodic ab initio quantum mechanical calculation including OH anharmonicity, Chem. Phys. Lett. 396 (2004) 308–315.
[50] H.G.M. Edwards, S.E.J. Villar, J. Jehlicka, T. Munshi, FT–Raman spectroscopic study of calcium-rich and magnesium-rich carbonate minerals, Spectrochim. Acta, Part A 61 (2005) 2273–2280.
[51] C. Paluszkiewicz, M. Gałka, W. Kwiatek, A. Parczewski, S. Walas, Renal stone studies using vibrational spectroscopy and trace element analysis, Biospectroscopy 3 (1997) 403–407.
[52] P. Battistoni, R. Boccadoro, F. Fatone, P. Pavan, Auto-nucleation and crystal growth of struvite in a demonstrative fluidized bed reactor (FBR), Environ. Technol. 26 (2005) 975–982.
[53] H. Huang, C. Xu, W. Zhang, Removal of nutrients from piggery wastewater using struvite precipitation and pyrogenation technology, Bioresour. Technol. 102 (2011) 2523–2528.
[54] P. Battistoni, P. Pavan, M. Prisciandaro, F. Cecchi, Struvite crystallization: a feasible and reliable way to fix phosphorus in anaerobic supernatants, Water Res. 34 (2000) 3033–3041.